HOW DOES A CRYOGENIC SYSTEM COPE WITH E-CLOUD INDUCED HEAT LOAD ?

B. Bradu, K. Brodzinski, G. Ferlin, CERN, Geneva, Switzerland

Abstract

Since 2012, the e-clouds produced by LHC beams are inducing significant dynamic heat loads on the LHC cryogenic system. These additional heat loads are deposited on beam screens where they must be properly extracted by the cryogenic system between 4.6 K and 20 K in order to ensure a stable beam vacuum and a good thermal barrier for superconducting magnets operated at 1.9 K. First, this paper describes how the cryogenic instrumentation located in the surrounding of the beam screens allows to measure the amount of power deposited by the beam and then to estimate the e-cloud contribution. Then, as this dynamic heat load induces fast transients on the cryogenic system, the standard feedback regulation techniques cannot be used anymore due to the slow response time of the cryogenic systems. Consequently, feed-forward controls based on beam information have been successfully setup from 2015 over the 485 beam screen regulation loops to guarantee optimal transients during the beam operation where significant heat load differences are observed all around the machine.

INTRODUCTION: LHC CRYOGENICS

LHC cryogenics is a large, complex and distributed system along the 27 km ring. Cryogenics must provide cryogenic conditions for many equipment in the LHC tunnel such as superconducting magnets, Distribution Feed Boxes (DFB) with their current leads, superconducting Radio-Frequency cavities, thermal shields and beam screens.

To fulfill all these requirements, eight cryoplants are installed around the LHC, sitting at points 18,2,4,6,8, see Fig. 1. Each cryogenic point is equipped with two cryoplants (except in P18/P2 where the two cryoplants are split for geographical reasons) to provide the cryogenic conditions to the two adjacent sectors [1].

One characteristic of the LHC cryogenics is its size and its access constraints. The cold mass is about 37000 $tons$ with an helium inventory of about 120 $tons$ stored in the magnets and in the cryogenic distribution line. Moreover, LHC is located in a confined area (tunnel) and the cryogenic distribution lines are long (3.5 km).

As the thermal transients mainly depends on the cold mass, the coolant mass, the surface of thermal exchange and the pipe diameters and lengths, the LHC cryogenic system response can be very slow and delayed. For instance, the time of flight for the helium supply at 4.5 K and 3 bar between the refrigerator and the end of the sector is about 8 hr, the time of flight for the helium return (3 K and 16 $mbar$) is about 20 min and the time of flight of beam screen helium return (20 K and 1.2 bar) is about 1 hr.

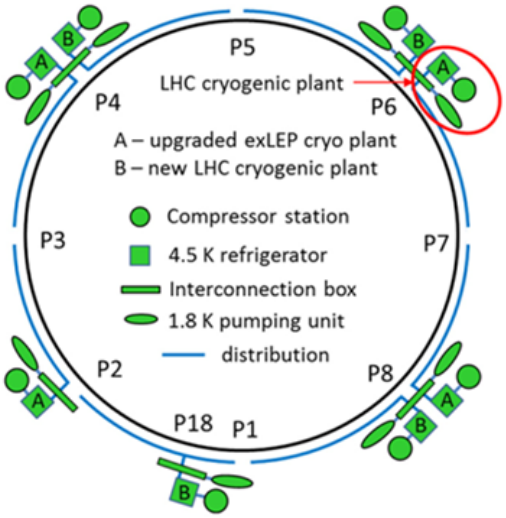

Figure 1: LHC cryogenics overview

All these considerations makes the LHC cryogenics very sensitive to the transients. Fortunately, most of the heat loads are static, but it remains significant dynamic heat loads which must be properly handled by the cryogenic system during the standard LHC operation (no beam - injection - ramp - stable beams - dump).

LHC dynamic heat loads

The main dynamic heat loads are either deposited in magnets at 1.9 K, either in beam screens between 4.6 K and 20 K. As the refrigeration power is not comparable for these two temperature levels, we will use equivalent isothermal power at 4.5 K as reference to be able to fairly compare the heat loads. The dynamic heat loads for the ultimate operation defined in the LHC design report are reported in Table 1 for a typical high-load sector as sector 1-2 [1].

As we can notice in Table 1, the main contributor in the dynamic heat loads is the electron-cloud component. Note that the Eddy current is also a large contributor but this heat load is present only during a short period of about 20 min during the magnet ramping and deramping. It is also important to note that dynamic heat loads applied on the 1.9 K magnet helium bath can benefit from the large superfluid helium heat capacity to smooth efficiently the transient whereas the transient is much more difficult to manage between 4.6 K and 20 K. Consequently, the dynamic heat load inducing the most significant impact on the cryogenic system is the electron-cloud, far away beyond other contributions.

Table 1: Equivalent isothermal dynamic heat loads at 4.5 K for one typical high load sector for ultimate operation.

Heat Load	Temperature	Cause	Heat Load Eq. @ 4.5 K	Remark
Resistive heating	1.9 K	Current in magnet splices	0.75 kW	Rise in 20 min
Eddy current	1.9 K	Current in magnet coils	2.5 kW	Only during ramp
Beam induced on magnets*	1.9 K	Beam and collisions	2.2 kW	Instantaneous
Synchrotron radiation	4.6 K – 20 K	Beam	0.8 kW	Instantaneous
Image current	4.6 K – 20 K	Beam	1.3 kW	Instantaneous
Electron-cloud	4.6 K – 20 K	Beam	5.0 kW	Instantaneous

*include beam gas scattering, photo e-cloud, collision debris in triplets, particle losses in DS.

Cryogenic beam screen circuits

Beam screens are located inside beam pipes and they are cooled by conduction via two cooling pipes of 3.7 mm diameter each, see Fig. 2. Beam screen cooling circuits are supplied by the Cryogenic Distribution Line (QRL) header C with supercritical helium at 3 bar and 4.6 K. After the the thermalisation of the magnet supports (magnet cold feet), an electrical heater (EH) is used to warm-up the helium in case of no beam-screen heat load when there is no beam-induced heating. Two helium circuits are then cooling in parallel the two beam screens in each aperture and the circuits are crossed at each magnet interconnection in order to homogenize the temperatures in case of asymmetrical heat loads between the two apertures. Finally, a control valve (CV) is managing the total flow at the outlet, ending to the QRL header D at 1.2 bar. The complete flow scheme and nominal temperatures and pressures are presented in Fig. 3 for a standard half-cell of 53 m which is repeated 485 times over the LHC ring.

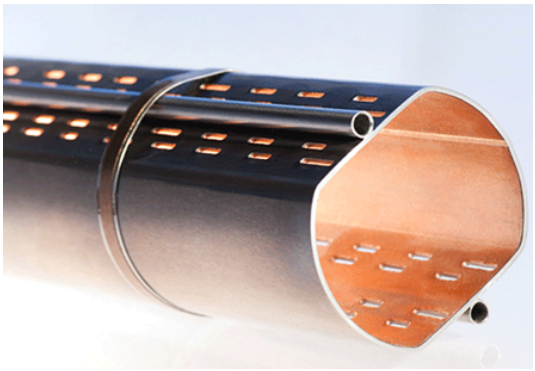

Figure 2: Beam screen with the associated cooling tubes

The temperature limits of the beam screen are defined to avoid thermo-hydraulic oscillations along the cooling pipes, to maintain stable vacuum in the beam pipe, to thermalize the current leads of the corrector magnets and to reduce beam-induced heat loads to the cold mass [2]. The minimum temperature is established between 6 K and 13 K, depending on the flow, to avoid thermo-hydraulic oscillations and the maximum allowed temperature is 40 K for 30 minutes to ensure ultra high vacuum conditions.

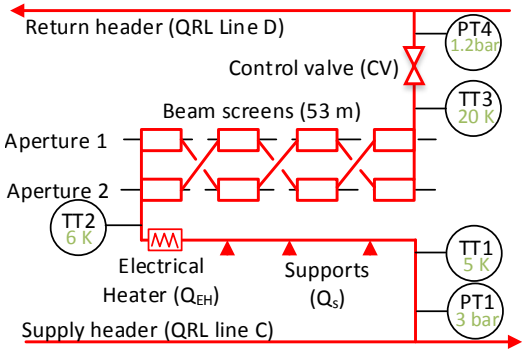

Figure 3: Beam screen cooling scheme with its associated instrumentation and typical values during beam operation

HEAT LOAD MEASUREMENTS

Standard half-cell heat load measurements

The beam screen heat load Q_{BS} can be simply calculated via an enthalpy balance on the beam screen cooling circuit as described in [8] using Eq. 1. Note that the sensor TT_2 is not reliable due to its proximity with the electrical heater and it is more accurate to perform the enthalpy balance on the complete cooling circuit betweeen the header C and the header D of the QRL, deducing the electrical heater power Q_{EH} and the static heat load $Q_s = 5\ W$. The enthalpies h are calculated using appropriated thermodynamic tables and the massflow $\dot{m}$ passing by the valve is computed using the Samson valve Eq. 2 where K_{vmax} represents the valve coefficient at maximum opening, R is the rangeability of the valve and CV is the valve position.

$$Q_{BS} = \dot{m} \cdot (h(P_3, TT_3) - h(PT_1, TT_1)) - Q_s - Q_{EH} \quad (1)$$

$$\dot{m} = 1.25 \cdot 10^{-5} \cdot \sqrt{P_3 \cdot \rho(P_3, TT_3)} \cdot \frac{K_{vmax}}{R} \cdot e^{CV \cdot \ln(R)} \quad (2)$$

The pressure before the valve P_3 is unknown and the pressure drop P induced by the frictions in the cooling tubes has to be computed using Eq. 3 ($P_3 = PT_1 - P$). fr is the friction coefficient computed using a valid correlation based on the Reynolds number, n_c is the total number of

cooling tubes in the circuits ($n_c = 4$ in the ARC), L is the circuit lentgh ($L = 53\ m$ in ARC), ρ is the helium average density in the circuit, D is the cooling tube diameter ($D = 3.7\ mm$) and S is the cooling tube cross section area.

$$P = fr \cdot \left(\frac{\dot{m}}{n_c}\right)^2 \cdot \frac{L}{\rho \cdot D \cdot S^2} \tag{3}$$

In this case, an algebraic loop is created as the massflow and the pressure drop are inter-dependent. This numerical problem can be easily solved by performing few iterations converging to the correct result.

Valve calibrations

The main source of error in the heat load calculation is coming from the valve massflow calculation in Eq. 2 in which the valve rangeability R is rarely well known. Consequently, some calibration measurements have to be done in order to estimate this parameter using the beam screen electrical heaters. The following sequence has been applied when there is no beam in the LHC on each beam screen valve:

- Open the valve at its usual opening when there is no beam ($\approx$ 30 %) and regulate the beam screen inlet temperature at 20 K using the electrical heater. The heater should be around 50 W.
- Open the valve at its maximal opening when there is beam ($\approx$ 65 %) and regulate the beam screen inlet temperature at 20 K using the electrical heater. The heater should be around 150 W.

Then, the rangeabilities for these two measurements are calculated to obtain $Q_{BS} = 0.0\ W$ from Eq. 1 and the average rangeability value R is taken to minimize the error over the valve opening range. The root mean square error ϵ_{rms} is then computed from Eq. 4 using the two errors ϵ_1 and ϵ_2 made when calculating Q_{BS} using Eq.1 with the average rangeability.

$$\epsilon_{rms} = \sqrt{1/2 \cdot (\epsilon_1^2 \quad \epsilon_2^2)} \tag{4}$$

Without calibration, taking the manufacturer rangeability, an rms error of about 15 % is observed whereas after the calibration process, the rms error is reduced to about 5 %.

Heat load measurement results

Once the valve calibration is achieved to reduce the error on the valve massflow computations, the different beam screen heat loads Q_{BS} can be calculated during beam operation. Fig. 4 and 5 show the results on the 485 beam screen circuits around the LHC for a typical beam operation at 50 ns and 25 ns.

At 50 ns, e-cloud heat loads are supposed negligible due to the significant bunch spacing and the heat loads are coming only from the synchrotron radiations and the image current. We observe an average of about 8 W per half-cell around the machine with a dispersion of about 1 W, which correspond precisely to the expected heat load for synchrotron radiations and image current for this fill using the usual scaling laws represented in Eq. 6 and 7.

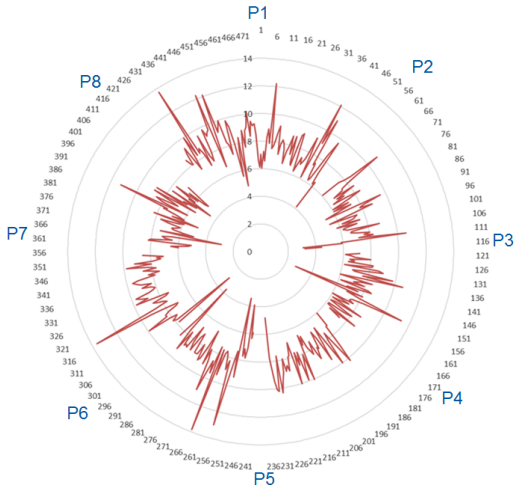

Figure 4: Beam screen heat load measurements at 50 ns during fill 5980 the 22nd July 2017. $nb = 1284\ bunches$; $I = 1.4 \cdot 10^{14}\ p\ /beam$; $E = 6.5\ TeV$.

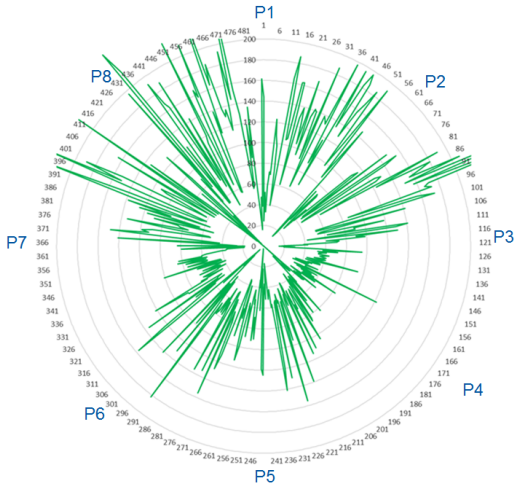

Figure 5: Beam screen heat load measurements at 25 ns during fill 6675 the 12th May 2018 (after scrubbing). $nb = 2556\ bunches$; $I = 3.0 \cdot 10^{14}\ p\ /beam$; $E = 6.5\ TeV$.

At 25 ns, e-cloud is expected to be the main contributor in the beam screen heat loads. We observe in this fill high heat load values along the machine, up to 200 W per half-cell but also a very high dispersion between half-cells and between sectors. A factor three can be observed between two sectors with a factor four between two adjacent half-cells whereas theoretically, all half-cells should show the same heat loads.

Instrumented half-cell heat load measurements

Four half-cells have been equipped with additional thermometers on the two beam screen cooling circuits between

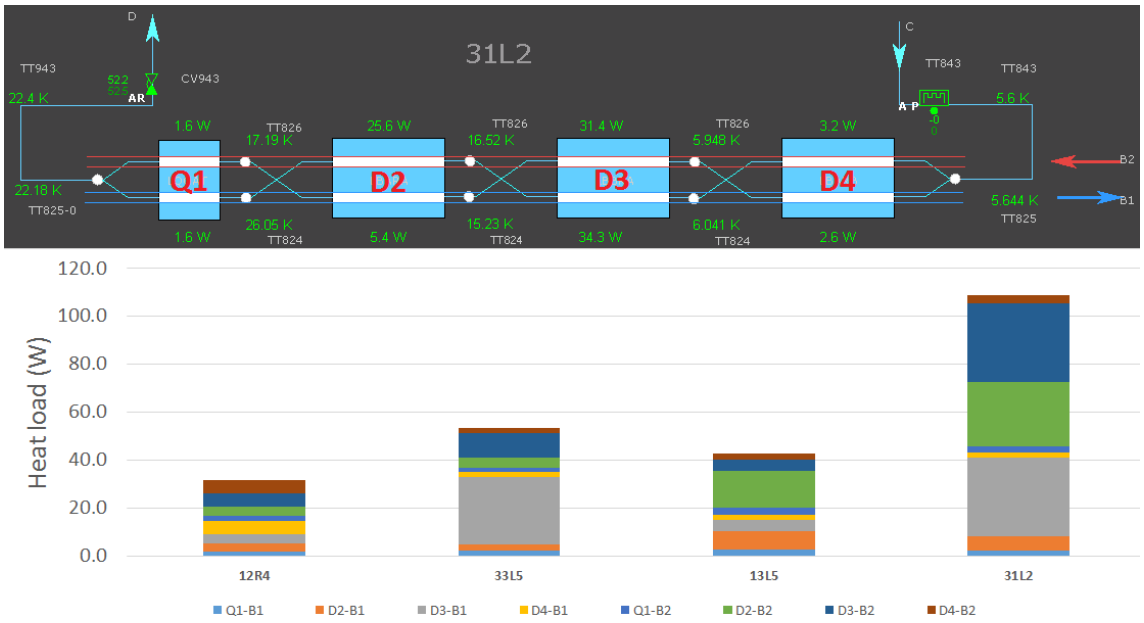

Figure 6: Typical scheme of an instrumented half-cell composed by one quadrupole $Q1$ and three dipoles $D2$, $D3$ and $D4$ (top). Summary of heat loads measured in each aperture ($B1$ and $B2$) of the four instrumented half-cells during Fill 6737 the 28^{th} May 2018 (bottom).

each magnets. These additional temperature sensors can be then used to perform independent enthalpy balances on each aperture for each magnet, giving a total of eight heat load measurements over the 53 m (two apertures on the four magnets), see Fig. 6 where one instrumented half-cell is represented with corresponding heat load measurements.

In the case of the instrumented half-cells, the thermal transients occurring on the beam screen after beam dumps when the heat load disappears can give useful information to estimate the possible heat load profiles along each aperture, see [9] for details. This analysis has been successfully done and is giving asymmetrical heat load distributions in the high load apertures.

HOW TO COPE WITH E-CLOUD TRANSIENTS ?

As described in the above sections, heat load transients induced by e-cloud can be a major issue for the LHC cryogenic system because of their high amplitude, their fast induced transient and their high versatility around the machine. In order to cope with e-cloud transients, two main paradigms have been established in the LHC cryogenic system management: *be prepared* and *start on time*.

Be prepared: pre-loading

The first intuitive action to be setup is the pre-loading of the cryogenic system using electrical heaters at appropriated power and locations when there is no beam. As the expected beam induced heat loads over the beam screens are about 3 kW @ 4.5 K on each LHC sector, such an equivalent power should be pre-loaded using different available electrical heaters when there is no beam. Two pre-loadings are performed in the machine:

- Pre-loading in the 4.5 K refrigerators with about 1.5 kW @ 4.5 K in the cold-box helium phase separator.
- Pre-loading in each of the individual beam screen cooling loop with about 50 W in each half-cell every 53 m. This pre-loading represent a total of about 1.5 kW @ 4.5 K on each sector.

Once this pre-loading is performed over the machine when there is no beam, the cryogenic control system has to remove progressively this pre-loading as function of the beam induced heat loads. The difficulty is then to perform this action in a synchronous manner with the beam parameters changes and the solution consists in starting on time.

Start on time: feed-forward control

First of all, the beam screen control scheme is composed by two independent feedback loops using two PID controllers as depicted in blue in Fig. 7:

- an outlet temperature controller (*PID1*) regulates the outlet temperature of the beam screen at 20 K using the control valve when there is no beam and at 22 K when there is beam with more than 600 bunches.
- an inlet temperature controller (*PID2*) regulates the beam screen inlet temperature at 13 K using the electrical heater located at the circuit entrance when there is no beam and at 6 K when there is a beam with more than 600 bunches;

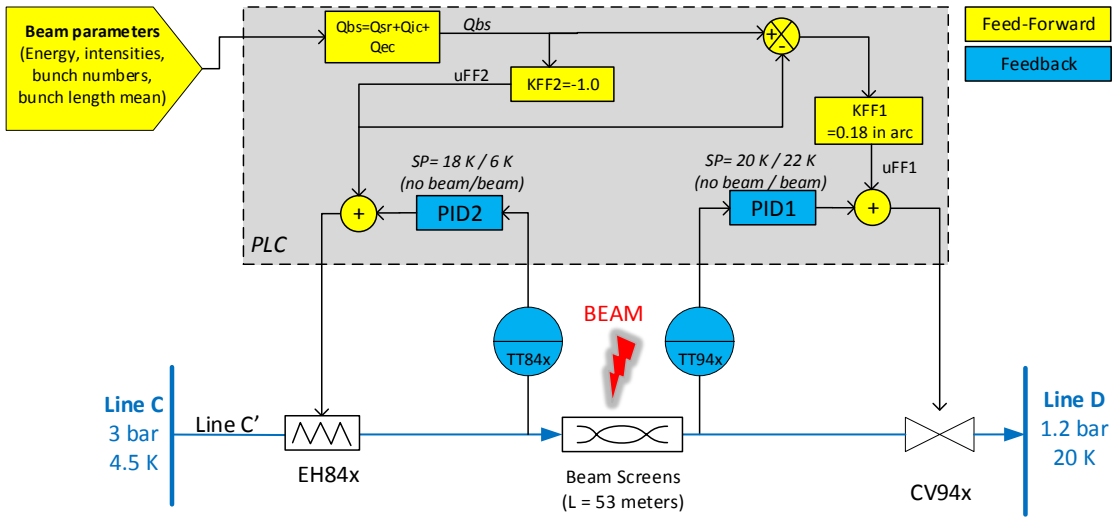

Figure 7: Beam screen control scheme embedding feedback and feed-forward control loops

These two feedback loops ensure a correct temperature distribution over the beam screen in steady-state with and without beams but they cannot manage properly the transients due to the large delays and time constants. Consequently, to start on time and to avoid over-shoots during fast transients, two feed-forward control loops have been setup in addition to the feedback loops as depicted in the yellow boxes of Fig. 7:

- First, the beam screen heat load Q_{BS} is estimated in real-time within the PLC, directly from the beam parameters (energy, intensities, bunch numbers and mean bunch length), see the next section for details.
- The electrical heater is then reduced proportionally with the estimated heat load until reaching 0.0 W.
- Then, if the estimated heat load becomes larger than the initial electrical heater value, the valve is opening proportionally with the additional estimated heat load to be compensated knowing the valve size.

As the delay between the beam-induced heat load and its effects on the beam screen outlet temperature is of the same order of magnitude than the effect of the valve action (around 10 minutes), this feed-forward action allows actuators to cancel the beam-induced heat load before any temperature overshoot happens. This feed-forward architecture is then optimal as all possible actuators are used to compensate the heat loads with shutting off completely the electrical heater when the heat load is maximum.

Beam induced heat load estimation

The deposited heat load on the beam screens Q_{BS} can be estimated from beam parameters doing the sum of the different contributions: synchrotron radiations Q_{sr}, image current Q_{ic} and electron cloud Q_{ec}, see Eqs. 5, 6, 7 and 8 where E is the beam energy, nb the number of bunches, Nb the number of protons per bunch, σ the mean bunch length and the different constants are summarized in Tab. 2.

$$Q_{BS} = Q_{sr} \quad Q_{ic} \quad Q_{ec} \tag{5}$$

$$Q_{sr} = Q_{sr0} \cdot L \cdot \left(\frac{E}{E_0}\right)^4 \cdot \left(\frac{Nb}{Nb_0}\right) \cdot \left(\frac{nb}{nb_0}\right) \tag{6}$$

$$Q_{ic} = Q_{ic0} \cdot L \cdot \sqrt{\frac{0.6 \cdot E \quad 2800}{E_0}} \cdot \left(\frac{Nb}{Nb_0}\right)^2 \cdot \left(\frac{nb}{nb_0}\right) \cdot \left(\frac{\sigma}{\sigma_0}\right)^p \tag{7}$$

$$Q_{ec} = \left[K_{eci} \cdot q_{eci} \cdot \left(1 - \frac{E - E_{inj}}{E_{ramp} - E_{inj}}\right) K_{ecr} \cdot q_{ecr} \cdot \left(\frac{E - E_{inj}}{E_{ramp} - E_{inj}}\right)\right] \cdot n_b \cdot \frac{Nb - Nb_t}{Nb_0 - Nb_t} \tag{8}$$

Due to the different electron cloud heat load values along the machine, three tuning parameters per half-cell are used in Eq. 8. q_{eci} and q_{ecr} represent respectively the electron cloud heat load value per bunch at injection energy (450 GeV) and after the ramp (6.5 TeV), and Nb_t represents the number of protons per bunch threshold where the electron cloud phenomenon appears. This parametrization is performed once a year using an automatic script with a reference fill to setup the 1455 parameters for all beam screen half-cells. Then, the two gains K_{eci} and K_{ecr} are initially

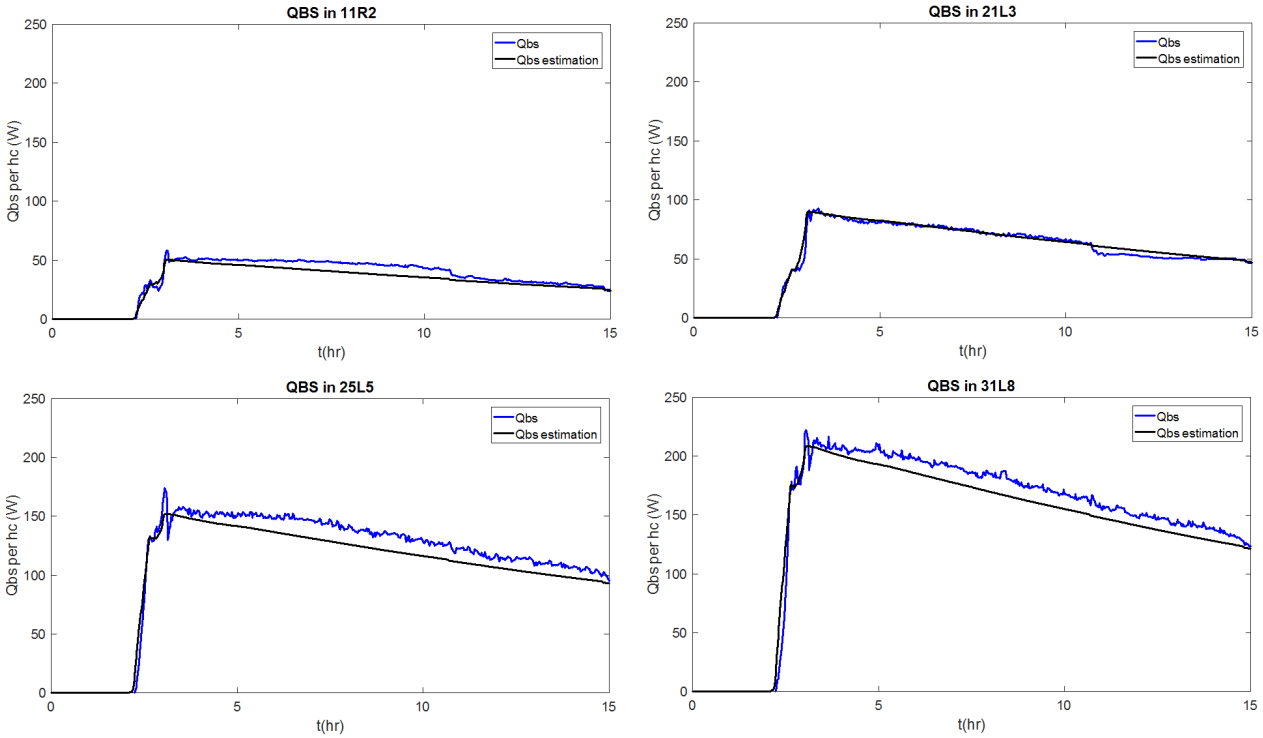

Figure 8: Beam screen heat load estimation compared to measurements on four different half-cells around the machine

equal to 1.0 and they can be tuned by cryogenic operators during the conditioning period in order to adjust easily and massively the electron cloud heat load estimations.

These equations allow us to reasonably estimate the deposited heat loads on the beam screens in all half-cells as we can see in Fig. 8 where a comparison between this model and measurements is shown on four different half-cells with different heat load values.

Table 2: LHC Beam screen heat load constants

Name	Description	Value
L	Beam screen length	53 m
E_0	Nominal energy	7 TeV
E_{inj}	Injection energy	0.45 TeV
E_{ramp}	Final energy after ramp	6.5 TeV
Nb_0	Nominal protons per bunch	$1.15 \cdot 10^{11}$
nb_0	Nominal bunch number	2808
σ_0	Nominal bunch length mean	1.06 ns
Q_{sr0}	Nominal synch. rad. load	0.165 W/m
Q_{ic0}	Nominal image current load	0.135 W/m
p	Bunch dependence factor	-1.5

Validation with dynamic simulations

In order to validate this control scheme including feedback and feed-forward control loops, several dynamical simulations were performed for the extreme cases, validating the different transient responses around the machine. To perform such simulations, a dynamic model of the cryogenic beam screen circuits developed on Ecosimpro some years ago have been re-used [6].

Fig. 9 and 10 show the simulation results for beam screen half-cells under high heat loads (peak of 230 W) and low heat loads (peak of 50 W) using only feedback loops (blue curves) and using feedback with feed-forward loops (red curves). The control scheme is perfectly fitting the requirements in both situations when the feed-forward loops are used, with a very small overshoot on the temperature outlet at 23 K during a short time and minimizing the necessary refrigeration power during the whole fill.

Results during LHC Run 2

Once the dynamic simulations proved the efficiency of the new proposed control scheme using feed-forward loops, the LHC cryogenic control system has been updated accordingly with a progressive deployment over the 485 beam screen cooling loops around the machine.

Fig. 11 is presenting the measurements over one high-load half-cell during a LHC nominal fill in May 2018. Results are very similar to the simulation performed for similar heat loads and the control scheme reacts as expected, correctly controlling the beam screen temperature and minimizing the refrigeration power variation.

Fig. 12 shows the same measurements but for a low-load half-cell during the same fill and the results are again in agreement with simulations demonstrating the efficiency on this control scheme for small heat loads as well.

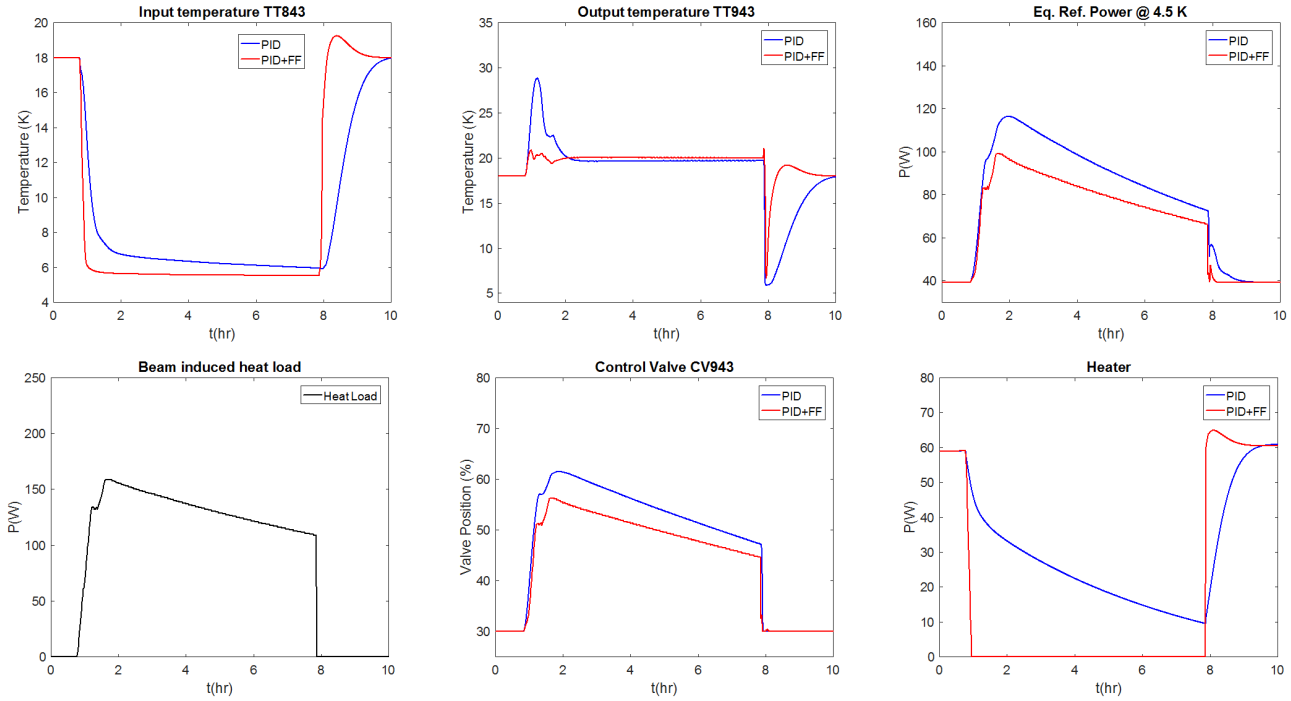

Figure 9: Beam screen dynamic simulation during a fill for a high heat load half-cell

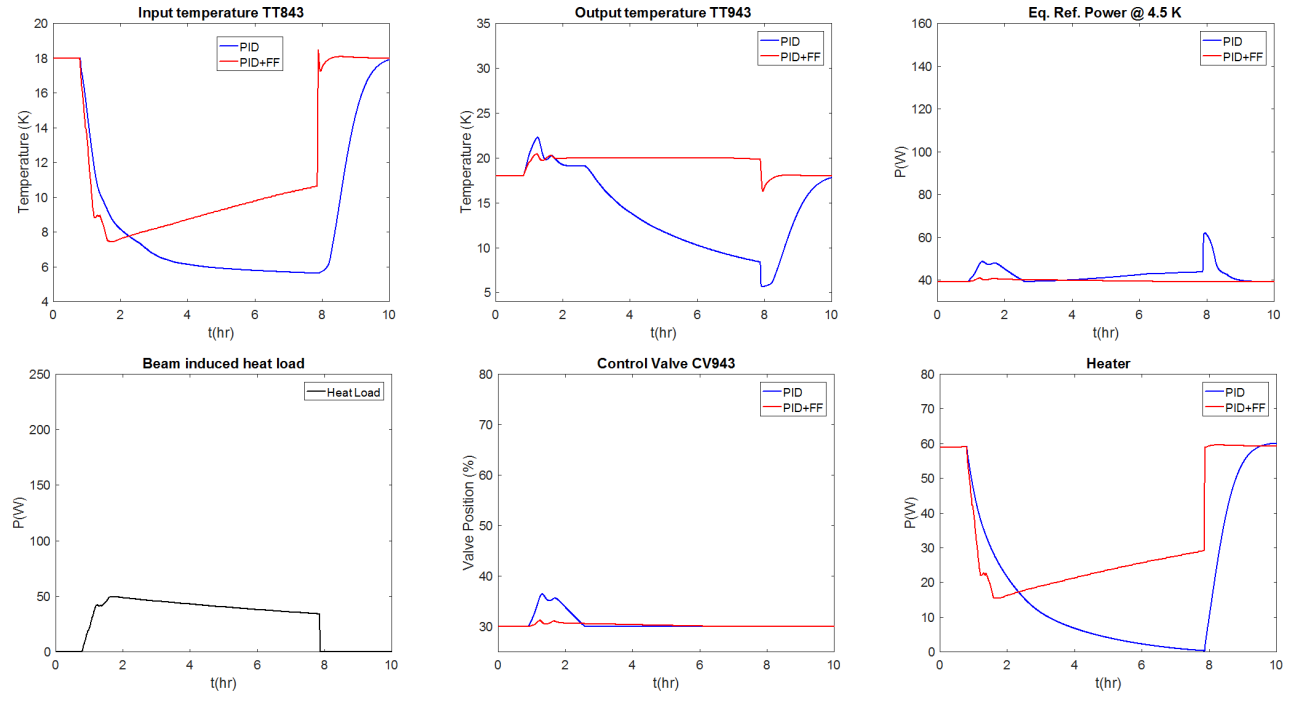

Figure 10: Beam screen dynamic simulation during a fill for a low heat load half-cell

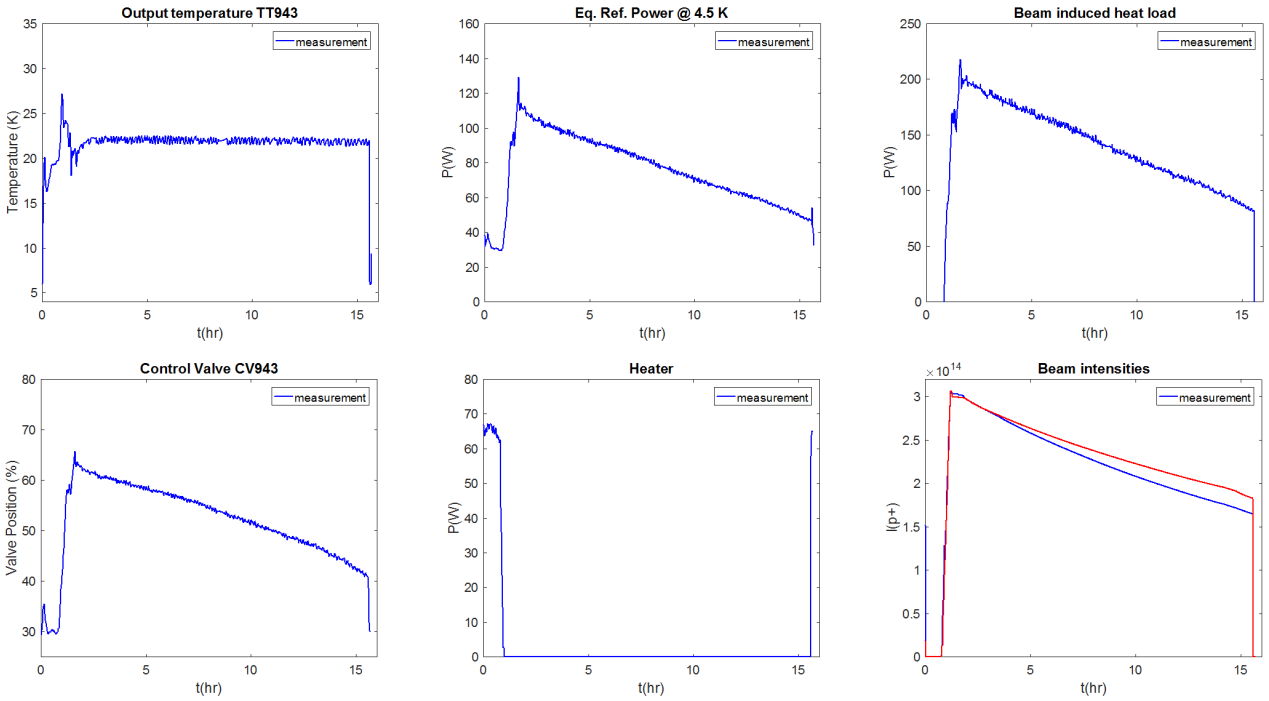

Figure 11: Beam screen measurements during the fill 6675 the 12th May 2018 for a high heat load half-cell

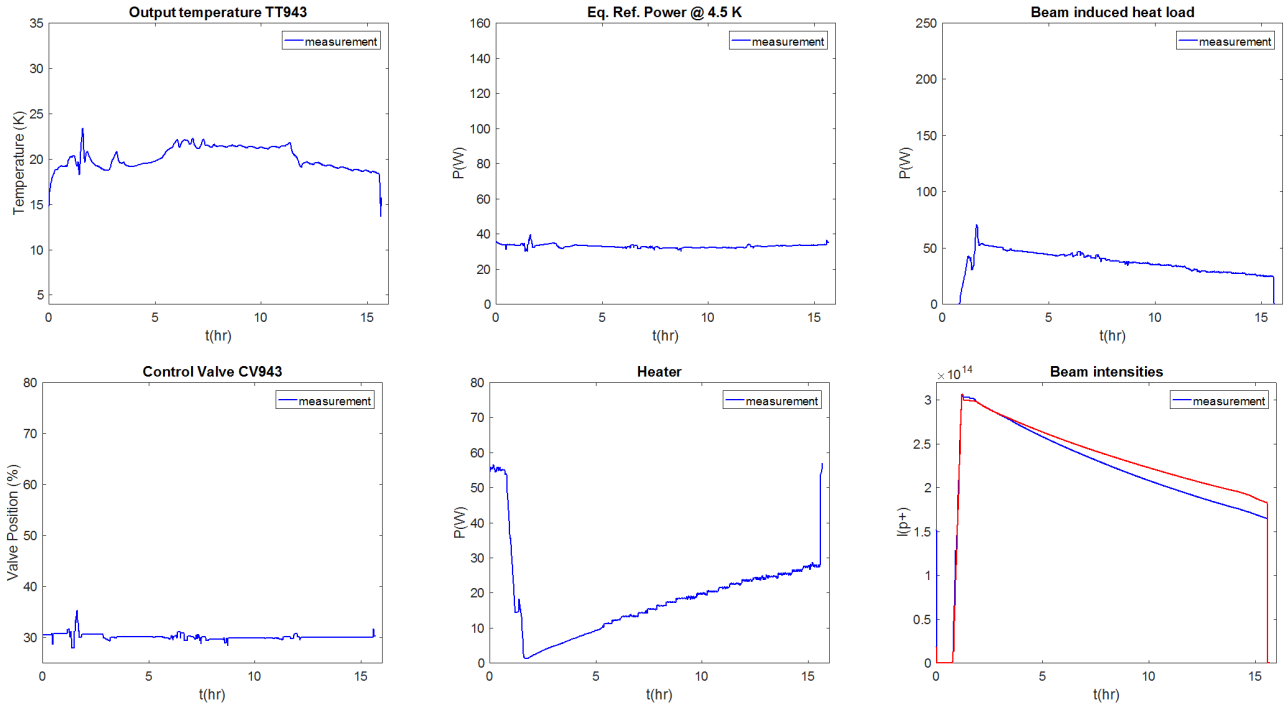

Figure 12: Beam screen measurements during the fill 6675 the 12th May 2018 for a low heat load half-cell

CONCLUSION

Since 2016, the Feed-Forward control scheme has been deployed and tuned over the 485 beam screen loops. This new control scheme proved its efficiency during the LHC Run 2, obtaining a cryogenic system able to cope with the important e-cloud induced heat loads. LHC cryogenic system is close to the optimal operation and it is not limiting the daily LHC operation as far as the total beam-induced heat loads are compatible with the available cooling power of refrigerators.

Nevertheless, LHC cryogenics is now approaching its hardware cryogenic capacity limit and heat loads cannot significantly increase in the coming years.

ACKNOWLEDGMENTS

This work has been possible tanks to the help of the cryogenics operation team, the control support teams, the CERN e-cloud experts and the collaboration of the LHC beam operation team.

REFERENCES

[1] O. Bruning et al., "LHC Design Report", CERN, Geneva (2004).

[2] V. Baglin, Ph. Lebrun, L. Tavian, R. van Weelderen, "Cryogenic Beam Screens for High-Energy Particle Accelerators", ICEC 24, Fukuoka, Japan (2012).

[3] G. Iadarola , G. Arduini, V. Baglin, H. Bartosik, J. Esteban Muller, G. Rumolo, E. Shaposhnikova, L. Tavian, F. Zimmermann , O. Domínguez "Electron Cloud and Scrubbing Studies for the LHC", IPAC 13, Shanghai, China (2013).

[4] K. Li, H. Bartosik, G. Iadarola, L. Mether, A. Romano, G. Rumolo, M. Schenk, "Electron cloud observations during LHC operation with 25 ns beams", IPAC 16, Busan, Korea (2016).

[5] B. Bradu, E. Rogez, E. Blanco, G. Ferlin, A. Tovar, " Beam screen cryogenic control improvements for the LHC run 2", ICEC 26, New-Delhi, India (2016).

[6] B. Bradu, E. Blanco, P. Gayet, "Example of cryogenic process simulation using EcosimPro: LHC beam screens cooling circuits", Cryogenics, 53:45-50 (2013).

[7] L. Tavian, "Performance limitations of the LHC cryogenics: 2012 review and 2015 outlook", LHC Beam Operation workshop, Evian, France (2012).

[8] K. Brodzinski, L. Tavian, "First Measurements of Beam-Induced Heating on the LHC Cryogenic System", ICEC 24, Fukuoka, Japan (2012).

[9] B. Bradu, K. Brodzinski, D. Delikaris, C. Garion, L. Tavian, "Heat load profile estimates on LHC beam screens by thermal transient analysis", ICEC 26, Oxford, United Kingdom (2018).

[10] E. Hatchadourian and Ph. Lebrun and L. Tavian, "Supercritical Helium Cooling of the LHC Beam Screens", ICEC 17, Bournemouth, United Kingdom (1998).